Real-time monitoring of bubble size distribution in a foam forming process

ANTTI KOPONEN, HANNU ELORANTA, ARI JÄSBERG, MARKUS HONKANEN, AND HARRI KIISKINEN

ABSTRACT: Foam forming is an intricate option to lessen fiber flocculation and to get better energy and water efficiency when making fiber-based products. Developed during the 1970s, this approach has recently received renewed attention, mainly because it also offers possibilities to widen the fiber-based product portfolios with novel and more valuable products. In addition to air content, bubble size is the most important property of foam. Foam quality control is essential for building real-world foam forming processes. In this work, we show how bubble size can be monitored with direct optical imaging in real time in real process conditions, and how such analysis helps adjust foam quality and discover process faults in foam forming.

Application: Foam quality control is essential for developing real-world foam forming processes. This study shows how bubble size can be monitored with direct optical imaging in real time under real process conditions.

Fiber flocculation is an enduring problem when fiber webs (e.g., paper or board) are made from wood fibers with water forming. Flocculation decreases the uniformity of the web, affecting most of its physical and optical characteristics. Fiber flocculation occurs primarily due to hydrodynamic forces acting on the fibers and mechanical interaction between them [1,2]. In conventional papermaking, the flocculation rate is lessened by using dilute enough fiber suspensions (to decrease the probability of fiber-fiber collisions) and by breaking the already-formed flocs by introducing turbulent energy to the fiber suspension—especially in the headbox. Different kinds of deflocculation agents are also commonly used. They either modify the surface properties of fibers, resulting in lower frictional forces between them, or increase the fluid viscosity, reducing the relative motion of the fibers and thus lowering the fiber crowding [3,4].

An intricate option to significantly lessen flocculation is to use foam as a carrier medium instead of water. Foam considerably decreases the mobility of fibers because it has orders-of-magnitude higher viscosity when compared to water. The fibers inside the foam are also locked between the bubbles that attach to the fiber walls and direct collisions between them become rarer. This approach to papermaking—foam forming—was under active development during the 1970s, but it was not widely adopted by the industry [5-9]. Foam forming has recently come back into the limelight, not only due to its improved formation and better energy and water efficiency, but also because it widens the product portfolio with novel and more valuable products [10-17].

Foam properties depend on many parameters, such as surfactant type and amount, foam generation setup (tank or in-line generation), introduced mixing energy, and the type and consistency of fibers [18-20]. Formation is typically improved when air content increases, (mean) bubble size decreases, or half-life increases [21]. Bubble size may also be inherited to the pore structure of the fiber sheet, improving the water removal in the press section [22,23]. The foam properties are thus key process variables in foam forming, and the ability to monitor and control them is of utmost importance for real-world processes.

Foams and bubbly liquids are used in many industrial applications, and the online measurement of the bubble size and the bubble size distribution has been studied in many scientific papers. A review on the various measurement methods is presented by Rodrigues and Rubio [24]. One way of classifying the methods is whether the sensors contacting the bubble phase are "intrusive" or "non-intrusive." The first category may present higher errors due to tool interference and may be also be problematic for real-world processes due to fouling. Another way of classifying the methods is whether the bubble size measurement is "direct" or "indirect." In the latter case, the measurement data is interpreted through a model, which often includes some assumptions and simplifications [25]. Obviously, the measurement method would preferably be direct and non-intrusive. Most available methods are either intrusive (wire mesh sensors [26]), indirect (conductivity measurements [27]; laser diffraction [28]), or both (dual-tip sensors [29,30]). Direct and non-intrusive methods include magnetic resonance imaging (MRI) [31] and optical imaging [32-33]. MRI is, in principle very, attractive, as it enables two-dimensional (2D) or three-dimensional (3D) tomographic imaging of the studied system. However, due to its high price and technical complexity, MRI is mainly used now for specific scientific studies in lab scale. Due to the rapid development of imaging technologies, image analysis, and computer

power, optical imaging is presently very popular. Its main disadvantage is the need for optical access for the image acquisition.

There are very few papers where the online measurement of foam properties has been addressed in real process conditions. Recently, the effect of foam quality on the sheet formation was studied in pilot conditions [21]. Foam was generated with a combination of tank and inline generation, which gave great flexibility in tuning the foam properties. When tank generation is used alone, the surfactant consistency must be high and the half-life is long. In such a case, offline measurement of foam properties may suffice. With inline generation, the surfactant levels can be very low. The half-life is then short, and online measurements are obligatory. Koponen et al. measured the air content online with a pressure loss difference between a horizontal and vertical pipe, and the half-life was measured automatically for foam samples taken continuously from the main flow [21]. The bubble size was measured online with a dedicated device, a foam monitoring system (Pixact Ltd.; Tampere, Finland), from a continuous sampling flow. This device has recently also been applied for the analysis of a bubbly liquid during oxygen delignification [34]. In this paper, we discuss this novel online measurement technique in detail and show its potential for adjusting foam quality and discovering process faults in foam forming.

MATERIALS AND METHODS

The foam monitoring system

Until the 1980s, the processing of the optical measurement data used to be time consuming, because the photographic direct optical measurement techniques relied on manual analysis [35,36]. Film cameras have since been replaced by charge-coupled device (CCD) and complementary metal oxide semiconductor (CMOS) cameras that can record gigabytes of measurement data per second directly in digital format. Present-day computational capacity enables processing of this data with complex image processing functions, even in real time. The complex processing of extensive sets of image-based measurement data makes it possible to quantitatively study the properties of the monitored system with high accuracy and reliability.

Direct optical imaging of bubble suspension followed by an image analysis to detect bubbles from the image data offers a very simple and accurate method to analyze foams and bubbly liquids. Such imaging techniques were introduced in 1980s [36-38], and the first online digital image analysis system for foams was presented by Sarker et al. [39] in 1998. After the introduction of high-resolution digital cameras, this technique has been developed intensively [40-44]. To date, direct optical imaging has been utilized in numerous scientific and industrial applications—mainly for bubbly liquids [45-51], but also for foams [52].

Basically, there are two options to illuminate the bubble suspension for imaging. In front illumination, the setup light comes from the direction of the camera. In this setup, reflections from the bubbles may decrease the image quality. Furthermore, due the curvature of the bubble surface, the periphery of the bubble is not that well defined and edge detection is challenging. In back illumination, the setup light comes from the back so that the camera sees the shadows of the bubbles. In this illumination setup, the bubble edges are sharp and well defined. This is essential if the measurement range extends to very small bubbles (i.e., diameter below 100 µm). As the bubble size distribution in foam forming typically peaks below 100 µm, back illumination is the preferred method.

In foam forming, the air content is typically high. This, in combination with the small bubble size, results in decreased light transmission through the foam due the high number of air-liquid interfaces. A very powerful light source is thus needed for transillumination. However, the air-liquid interfaces also make the foam act like a diffuse medium, which leads to high-quality images of the bubbles.

The Foam Monitoring (FM) system combines in-situ optical process microscopy and advanced image analysis algorithms to provide real-time measurement data of bubbles in wet and dry foams. Imaging of the foam is carried out continuously in

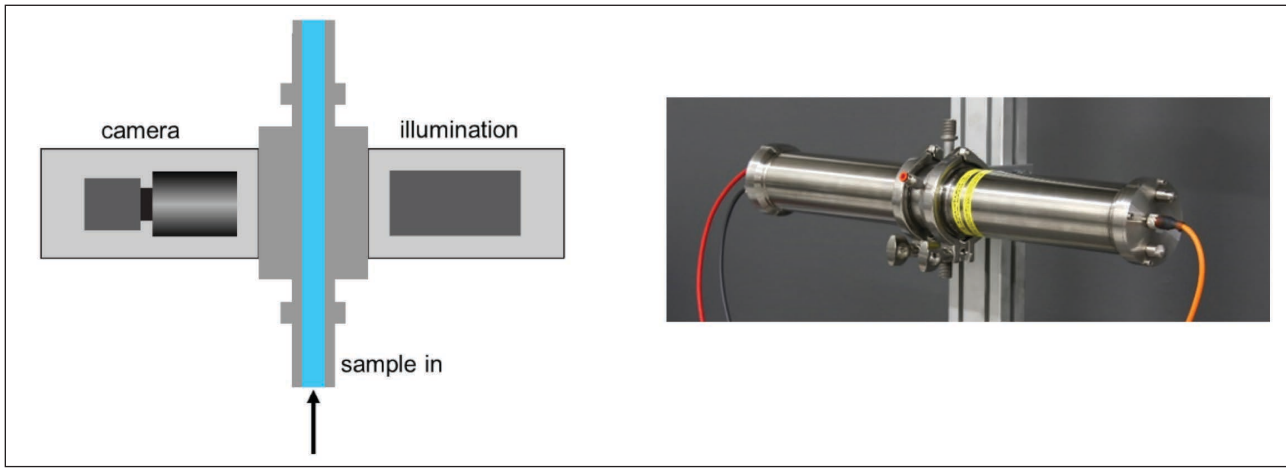

1. Operating principle of the Foam Monitoring (FM) system (left), and the flow-through cuvette used for imaging (right).

the flow-through cuvette (**Fig. 1**). The foam is flowing through the imaging section in which the round sampling line is converted into a 3 mm × 25 mm rectangular cross section. The cross-sectional area is the same as in the supply line. The thickness of the trans-illuminated foam layer is thus 3 mm. As the bubbles are rather small and the shear forces are low in the flow-through cuvette, the bubbles are almost spherical. The cuvette can be installed directly to a process pipeline or to a dedicated sampling line. The cuvette is equipped with an automatic washing system.

Images of bubbles are acquired with a CCD camera (ImperX IGEV-B1410M, ImperX; Boca Raton, FL, USA). Only the latest developments in LED and laser technology have created light sources suitable for in-situ transillumination of foams. In this case, the transillumination of the foam is carried out by a diode laser illumination unit. This unit enables very high optical power to be focused to the camera imaging area. The energy of the light pulse used for imaging of the foam is in the range of 10–1000 mJ, depending on the foam quality. The light energy is automatically adjusted by the measurement system to produce an optimal gray scale histogram in the images. The system produces blur-free images at the rate of 10 images per second with image dimensions of 4.5 mm × 3.4 mm and pixel size of 3.2 µm. Example images acquired by the FM system are shown in **Fig. 2**.

An image analysis algorithm has been utilized to detect bubbles and measure their diameter. Gas bubbles appear as dark rings on a bright background, as shown in **Fig. 3**. The outlines of the rings (i.e., the bubble edges) are detected with an iterative least squares circle fit, which validates the edges based on their length and greyscale curvature. In order to select valid (i.e., circular or nearly circular) edges, at least 50% of the bubble outline must be detected—shorter edge segments are rejected. Both the curvature of detected edges and their length are compared to the perimeter of a circle with equal diameter. High-precision sub-pixel fitting method was not necessary in the current application and the accuracy of the outline detection was limited to the pixel size (i.e., 3.2 µm). However, it is also possible to locate the gas-liquid interfaces with sub-pixel accuracy [54].

In this work, the (area-weighted) bubble size distribution and Sauter mean diameter of the bubbles, provided by the FM system, were averaged over a 60 second period (i.e., over 600 images). Sauter mean diameter is defined as:

$$D_{32} = \frac{\sum_{i=1}^{N} n_i d_i^3}{\sum_{i=1}^{N} n_i d_i^2}, \qquad (1)$$

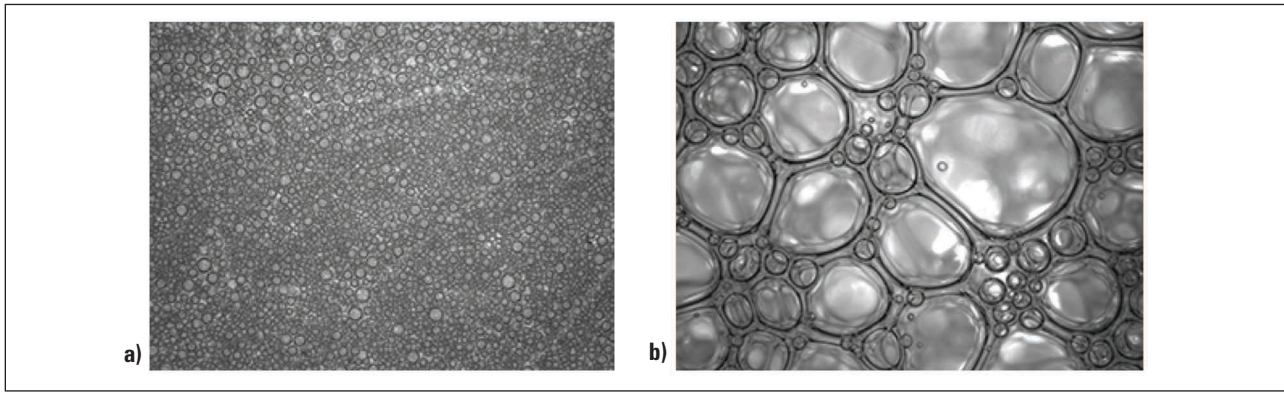

2. Examples of images taken with the FM system: a) wet foam, and b) dry foam. The image height is 3.4 mm and the pixel size is 3.2 µm. Note that foams are called "bubbly liquids" when air content is smaller than 65%, "wet" when air content is between 65% and 85%, and "dry" when air content is more than 85% [53].

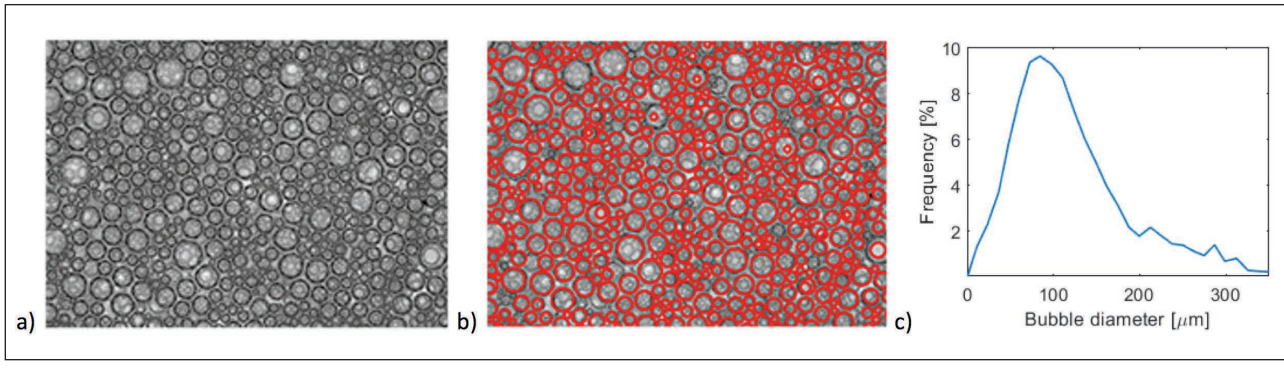

3. a) Example of a raw image of foam; b) bubbles found by the bubble detection algorithm; and c) the obtained area-weighted bubble size distribution. The Sauter mean diameter is 120 µm. The image height is 3.4 mm and the pixel size is 3.2 µm.

where n_i and d_i are, respectively, the number and diameter of bubbles in a particular size fraction. Sauter mean diameter reflects the size of identical spherical bubbles—a system of which has the same total area and total volume as the system of the polysized bubbles [55]. The total surface energy of the monosized bubbles is then equal to the total surface energy of polysized bubbles. As surface energy is a fundamental quantity for foams, Sauter mean diameter is widely used for describing the mean size of bubbles. Thus, in the following, the Sauter mean diameter is called simply mean diameter, and it is denoted by D.

EXPERIMENTAL

Laboratory-scale testing

As a laboratory-level test case, we analyzed foam generated by pumping a mixture of sodium dodecyl sulfate (SDS) solutions and air through a sawtooth profiled turbulence generator installed in a pipe having a diameter of 33 mm. The foam density was approximately 400 g/m³. In **Fig. 4**, the measured mean bubble diameter, D, is shown as a function of the volumetric flow rate of water, Q, for three SDS dosage levels. The mean bubble diameter is shown to decrease with increasing SDS dosage, as well as with increasing volumetric flow rate through the turbulence generator (i.e., increasing energy input to the flow). The mean bubble diameter was found to be given with a good accuracy by the simple formula:

$$D = D_0 + \frac{k}{Q^{1.5}} \qquad (2)$$

where D_0 and k are fitting parameters for different SDS levels. The obtained values for D_0 and k are shown in **Table I**. Notice that parameter D_0 is the limiting bubble size at very high flow rates. **Figure 4** suggests that there is also a limiting value for the bubble size with an increasing SDS dosage level.

Pilot-scale testing

The pilot scale trials presented in the following description were performed in VTT's pilot environment (VTT Technical Research Centre of Finland Ltd.; Jyväskalä, Finland) by using a long vacuum-assisted forming board. The used furnish was bleached unrefined softwood chemical pulp. SDS was mainly used as the surface-active agent. No retention chemicals were used during the trial. The foam was generated with a combination of tank and inline generation. The foam density, ϱ, varied between 250 and 700 kg/m³ and the share of the injected air in inline generation, S, of the total amount of air in the foam varied between 0 and 0.8. SDS concentration varied in the range of 10–180 ppm. Low doses of SDS were typically compensated by increasing the share of the injected air. The inline generation was performed by dividing the foam before the headbox into 30 tubes, including a sawtooth profiled turbulence generator with air injection. One of the tubes was connected to a sampling device that measured the bubble size

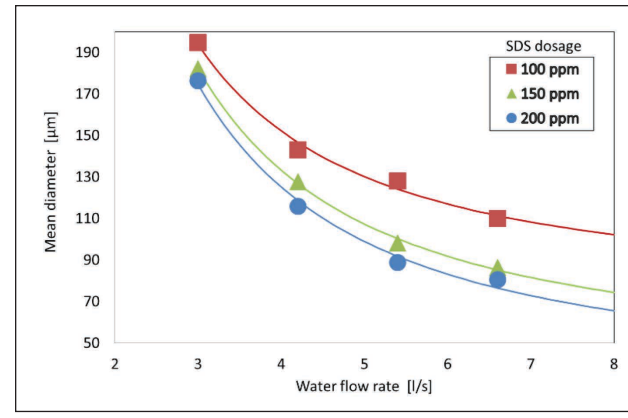

4. The measured bubble diameter for foam generated by pumping a mixture of water, air, and sodium dodecyl sulfate (SDS) through a turbulence generator. The solid lines are given by Eq. 2, with the parameter values shown in Table I.

SDS Dosage, ppm	100	150	200
D_0, µm	75	42	33
k, µm • (l/s)$^{1.5}$	620	730	740

I. The values of the fitting parameters D_0 and k in Eq. 1 for different sodium dodecyl sulfate (SDS) dosage levels.

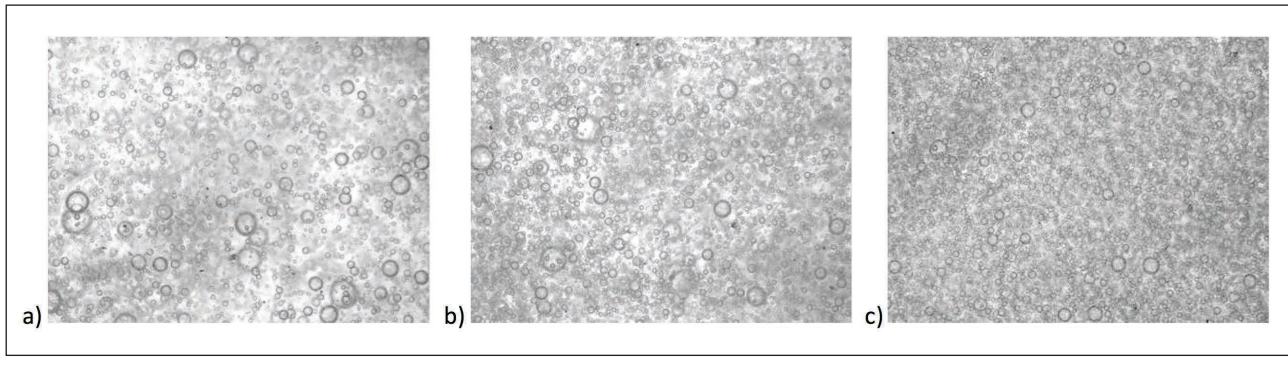

5. Sample images of foam during an addition of foaming agent (Tween): a) The feed is started with a mean diameter of D = 100 µm; b) 3 min later, the mean diameter has dropped to D = 75 µm; and c) the situation 8 min from the start. The foam has reached a steady bubble size distribution with a mean diameter of D = 55 µm.

with the FM device and measured half-life with a fully automatic drainage analyzer. Foam density was measured online with a pressure loss difference between a horizontal and vertical pipe. The target basis weight of the final paper sheets was 70 g/m². Fiber consistency varied for foam between 0.7% and 1.8%, while for the water reference, it was 0.5% in most cases. The machine speed varied between 400 and 800 m/min. The press section consisted of a 1-nip shoe press having a 350 mm extended nip. After the wet pressing, the paper web was reeled and sheet samples were collected and dried for optical (specific) formation analysis. The pilot scale trials and the various measurement methods have been discussed in detail by Koponen et al. [21].

Figure 5 shows three sample images of foam during an addition of a foaming agent (Tween 20, polyoxyethylenesorbitan monolaurate; Sigma-Aldrich, St. Louis, MO, USA) in VTT's pilot environment, and **Fig. 6** shows the corresponding bubble size distributions. The foam was generated by mixing in a pulper in the approach system, and there was a delay in the response of the state of foam to the surfactant dosage. After the dosage, foam reached a new stable state in 8 min, during which the mean diameter of bubbles decreased from 100 µm to 55 µm.

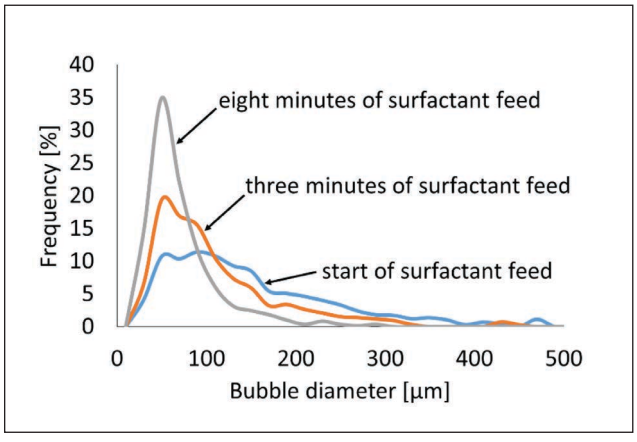

6. Bubble size distributions of the three foams shown in Fig. 5.

The most important properties of foam in forming are density ρ and bubble size *D*. Another relevant property of foam is drainage rate (or half-life), but with a given dosage of surfactant, it cannot be controlled independently of density and bubble size. In [21], SDS content c_{SDS} and share of injected air *S* were clearly found to be the most important process parameters determining the foam properties. **Figure 7** shows the foam density and the bubble size for all the pilot trial points as a function of SDS content and share of injected air. We see in Fig. 7a that foam density decreases with increasing SDS content and increasing share of injected air. Decreased SDS content can thus be compensated with higher share of injected air to keep the foam density constant. Figure 7b shows that bubble size decreases with increasing SDS content and decreasing share of injected air. The amount of turbulent energy seems to be too small with the current inline geometry to break the injected air to as small bubbles as the foam generation in tank does.

Koponen et al. [21] suggested the formulae $\rho = \alpha c_{SDS} + \beta S + \gamma$ and $D = \alpha' S/c_{SDS} + \beta'$ for the foam density and the mean diameter, respectively (here, α, β, γ, α' and β' are regression coefficients). It is thus possible, in principle, to adjust both the bubble size and foam density by choosing proper values for *S* and c_{SDS}. The obtained foams, however, are not necessarily identical. **Figure 8** shows the normalized standard deviation, $\bar{\sigma}$, of the bubble size as a function of mean diameter for all the trial points; the share of injected air is also shown. We see that $\bar{\sigma}$ tends to increase with increasing bubble size and that $\bar{\sigma}$ may differ as much as a factor two between two foams. **Figure 9** shows bubble size distributions for the foams marked in Fig. 8 with letters "a",

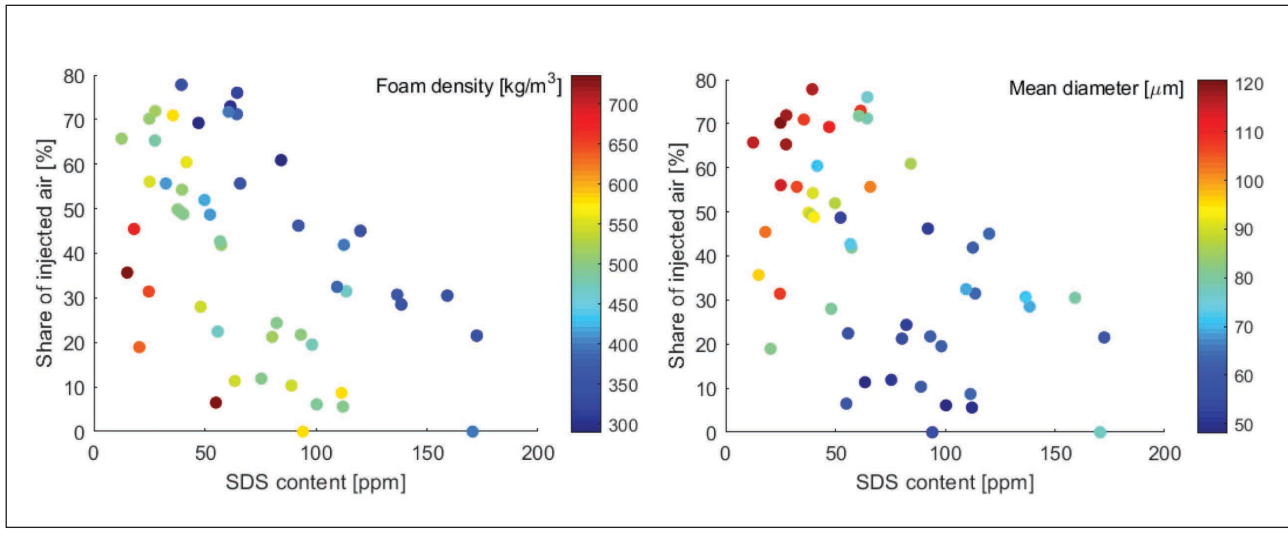

7. a) SDS content, share of injected air, and foam density for all trial points. Foam density increases with increasing SDS content and increasing share of injected air; b) SDS content, share of injected air, and mean diameter for all trial points. Bubble size decreses with increasing SDS content and decreasing share of injected air.

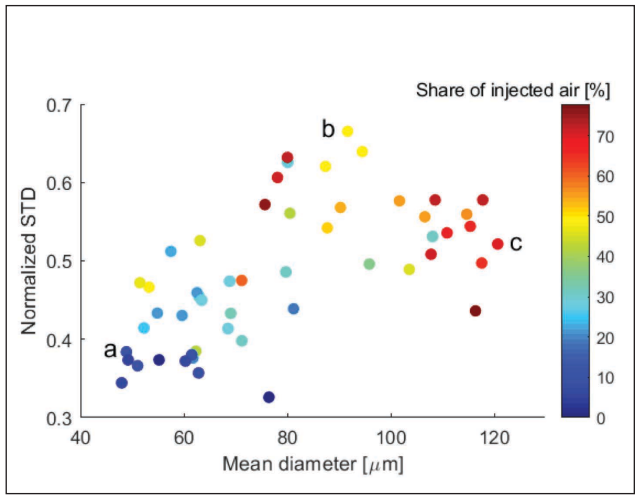

8. The normalized standard deviation of the bubble size as a function of mean diameter. The share of injected air is shown with colors. The normalized standard deviation is seen to increase with increasing share of injected air. The letters "a", "b" and "c" refer to the bubble size distributions shown in Fig. 9.

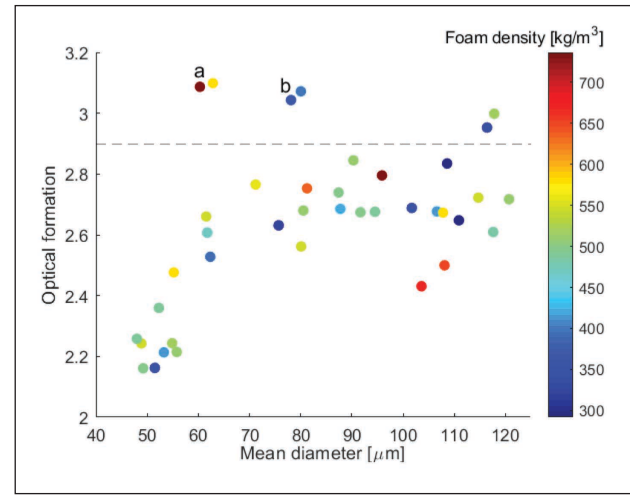

10. Optical formation, bubble size and density for all trial points. The dashed line indicates the best formation, 2.9, obtained with water forming. The points marked with "a" had high shear of injected air and very high crowding number. The points marked with "b" had high normalized standard deviation $\bar{\sigma}$ of the bubble size indicating problems with foam quality.

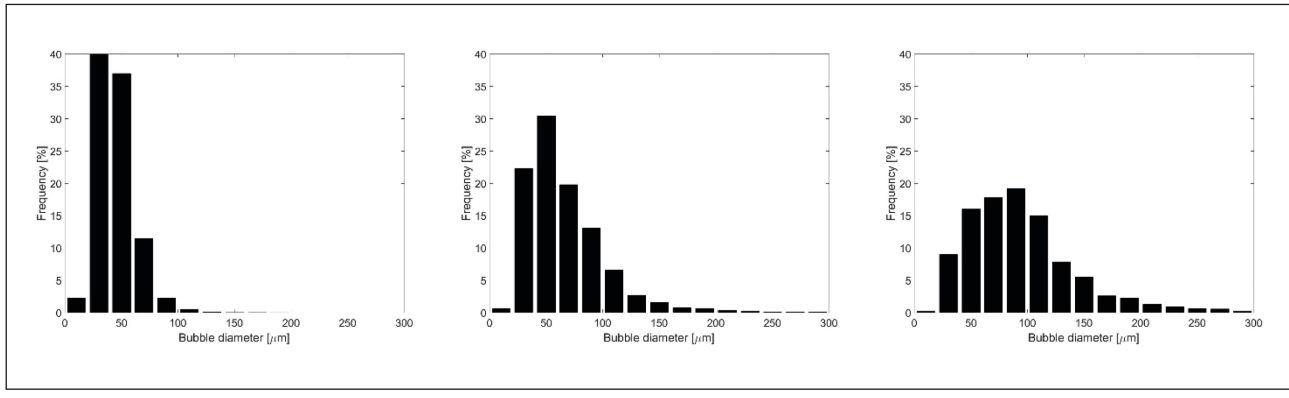

9. The bubble size distributions for the foams marked in Fig. 8 with letters "a" (D = 49 µm, $\bar{\sigma}$ = 0.37, S = 0.06); "b" (D = 92 µm, $\bar{\sigma}$ = 0.67, S = 0.50); and "c" (D = 121 µm, $\bar{\sigma}$ = 0.52, S = 0.70).

"b", and "c". We see in Fig. 9 that the foam generated almost purely with tank generation (S = 0.06) has a very narrow, approximately Gaussian, bubble size distribution, and there are few bubbles with a diameter higher than 100 µm. We also see that when the share of injected air is significant, the bubble size distributions are lognormal, they have long tails, and the size of individual bubbles may exceed 300 µm. There are thus both qualitative and quantitative differences in the bubble size distributions of foams made with tank and inline generation.

In **Fig. 10** the formation of paper samples, bubble size, and the foam density are shown. The formation of water-formed samples varied between 2.9 and 3.5, thus being clearly worse than for most foam-formed samples. We see in Fig. 10 that best formation is obtained with small bubbles and that formation is rather similar when bubble size is higher than 80 µm. We also see that there are a few outliers than do not follow the general trend. The two points marked with "a" had very high crowding numbers (115 and 148), which, together with the rather high foam density, may explain the behavior. The points marked with "b", on the other hand, had high normalized standard deviation $\bar{\sigma}$ of the bubble size ($0.6 < \bar{\sigma}$) indicating possible problems with the foam quality. The formation data and its dependence on various process parameters, such as foam density, share of injected air, and crowding number, have been discussed in more detail in [15,21].

CONCLUSIONS

A camera-based online measurement system has been installed in a pilot-scale foam forming environment to monitor the bubble size distribution online. The measurement system has been found to be a robust tool for monitoring the foam quality in a headbox. After installation in 2014, the monitoring system has been used in all the foam forming trials in the pilot environment.

In process conditions, the measurement information on the size of the bubbles and foam homogeneity helps to tune

the foam quality and optimize, control, and troubleshoot the process based on real-time statistics. Moreover, the available live image view provides the operator with real-time visual information on the process, making, for example, the detection of potential process disturbances (e.g., excessive large air bubbles) possible. In addition, the measured bubble size data can be saved for later retrieval and analysis together with the relevant properties of the final product.

According to the pilot scale experiments, the bubble size correlates with the optical formation of the final product—smaller bubbles usually result in better formation. This limits the share of injected air for the current inline foam generation, as it tends to generate foams with bigger bubbles and wider size distributions with a high share of injected air. It is likely that the bubble size and distribution width could be decreased by increasing turbulent energy (e.g., by making the turbulent generator longer).

If the raw material composition is otherwise fixed, the properties of fibrous foam can be affected by the selection of surfactant, surfactant dosage, and intensity and time of mixing while generating the foam. In particular, when inline foam generation technology is used with small dosages of surfactant, there is a risk that air and liquid phases separate before forming on the web. This may lead to, for example, pinholes in the final product. However, there is currently no online method available for measuring the surfactant dosage. This makes the combination of an optical bubble size monitoring system and a foam density measurement device obligatory for monitoring an industrial scale foam process—especially if an inline foam generation technology is used. **TJ**

ABOUT THIS PAPER

Cite this article as:
Koponen, A., Eloranta, H., Jäsberg, A., et al., *TAPPI J.* 18(8): 487(2019). https://doi.org/10.32964/TJ18.8.487

DOI: https://doi.org/10.32964/TJ18.8.487

ISSN: 0734-1415

Publisher: TAPPI Press

ACKNOWLEDGEMENTS

This work was performed in Foam Forming Program—towards industrial scale applications, which is funded by European Regional Development Fund (ERDF, No A70131), VTT Technical Research Centre of Finland Ltd., and 20 industrial partners.

LITERATURE CITED

1. Mason, S., *Pulp Pap. Mag. Can.* 87(13): 96(1954).
2. Schmid, C., Switzer, L., and Klingenberg, D., *J. Rheol.* 44(4): 781(2000). *https://doi.org/10.1122/1.551116*.
3. Yan, H., Lindström, T., and Christiernin, M., *Nord. Pulp Pap. Res. J.* 21(01): 36(2006). *https://doi.org/10.3183/npprj-2006-21-01-p036-043*.
4. Zhao, R., and Kerekes, R., *Tappi J.* 76(2): 183(1993).
5. Radvan, B. and Gatward, A., *Tappi* 55(5): 748(1972).

ABOUT THE AUTHORS

This paper discusses a measurement method used in our foam forming studies and also in our published studies. The most difficult aspect of the present study was to develop a robust measurement method for bubble size that also works in a real-world environment.

Through this study, we discovered the dependence between foam properties and end-product quality. The most interesting finding was the bubble size distributions that were composed while simultaneously using tank and online foam generation.

For mills that plan to use foam forming, this measurement method will be necessary. Our next step is to find new applications for the imaging technology used here.

Koponen is principal scientist, Jäsberg is senior scientist, and Kiiskinen is principal scientist at VTT Technical Research Centre of Finland Ltd. in Jyväskylä, Finland. Eloranta is managing director and Honkanen is head of PCM & PBM Technologies at Pixact Ltd., Tampere, Finland. Email Koponen at Antti.Koponen@vtt.fi.


Koponen


Jäsberg


Kiiskinen

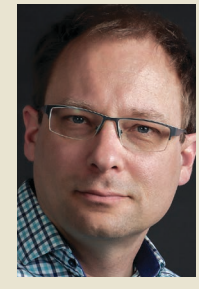
Eloranta

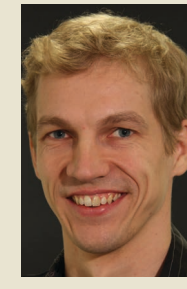
Honkanen

6. Tringham, R., "New developments in the Radfoam process," *Pap. Technol.* 15(5): 288(1974).
7. Smith, M. and Punton, V., *Pulp Pap. Can.* 76(1): 55(1975).
8. Punton, V., "Fiber distribution in foam and foam-laid paper," *Int. Pap. Phys. Conf.*, 1975, pp. 135-39.
9. Punton, V., "The use of an aqueous foam as a fiber-suspending medium in quality papermaking," in *Foams, Proceedings of a Symposium Organized by the Society of Chemical Industry, Colloid and Surface Chemistry Group* (R.J. Akers, Ed.), Society of Chemical Industry, London, 1975.
10. Hellén, E., Jetsu, P., and Lehmonen, J., *Pap. Technol.* 54: 10(2013).
11. Poranen, J., Kiiskinen, H., Salmela, J., et al., "Break-through in papermaking resource efficiency with foam forming," *TAPPI PaperCon*, TAPPI Press, Peachtree Corners, GA, USA, 2013.
12. Lappalainen, T., Salminen, K., Kinnunen, K., et al., *Nord. Pulp Pap. Res. J.* 29(04): 689(2014). https://doi.org/10.3183/npprj-2014-29-04-p689-699.
13. Torvinen, K., Lahtinen, P., Kiiskinen, H., et al., "Bulky paper and board at a high dry solids content with foam forming," *TAPPI PaperCon*, TAPPI Press, Peachtree Corners, 2015.
14. Alimadadi, M. and Uesaka, T., *Cellulose* 23: 661(2016). https://doi.org/10.1007/s10570-015-0811-z.
15. Koponen, A., Torvinen, K., Jäsberg, A., et al., *Nord. Pulp Pap. Res. J.* 31(2): 239(2016). https://doi.org/10.3183/npprj-2016-31-02-p239-247.
16. Bunker, D., Cecchini, J., Hietaniemi, M., et al., "Foam forming technology folding box board focused developments," *TAPPI PaperCon*, TAPPI Press, Peachtree Corners, 2017.
17. Liu, Y., Kong, S., Xiao, H., et al., *Carbohydr. Polym.* 182(June 2017): 92(2018). https://doi.org/10.1016/j.carbpol.2017.10.078.
18. Al-Qararah, A., Hjelt, T., Koponen, A., et al., *Colloids Surf., A* 436: 1130(2013). https://doi.org/10.1016/j.colsurfa.2013.08.051.
19. Mira, I., Andersson, M., Boge, L., et al., *Nord. Pulp Pap. Res. J.* 29(4): 679(2014). https://doi.org/10.3183/npprj-2014-29-04-p679-689.
20. Al-Qararah, A., Hjelt, T., Koponen, A., et al., *Colloids Surf., A* 467: 97(2014). https://doi.org/10.1016/j.colsurfa.2014.11.034.
21. Koponen, A., Jasberg, A., Lappalainen, T., et al., *Nord. Pulp Pap. Res. J.* 33(3): 482(2018). https://doi.org/10.1515/npprj-2018-3051.
22. Al-Qararah, A., Ekman, A., Hjelt, T., et al., *Colloids Surf., A* 482: 544(2015). https://doi.org/10.1016/j.colsurfa.2015.07.010.
23. Koponen, A., Ekman, A., Mattila, K., et al., *Transp. Porous Media* 117(2): 247(2017). https://doi.org/10.1007/s11242-017-0831-2.
24. Rodrigues, R. and Rubio, J., *Miner. Eng.* 16(8): 757(2003). https://doi.org/10.1016/S0892-6875(03)00181-X.
25. Jamshidi, N. and Mostoufi, N., *Biochem. Eng. J.* 125: 212(2017). https://doi.org/10.1016/j.bej.2017.06.010.
26. Prasser, H.-M, Scholz, D., and Zippe, C., *Flow Meas. Instrum.* 12(4): 299(2001). https://doi.org/10.1016/S0955-5986(00)00046-7.
27. Xie, W., Neethling, S., and Cilliers, J., *Chem. Eng. Sci.* 59(1): 81(2004). https://doi.org/10.1016/j.ces.2003.09.020.
28. Couto, H., Nunes, D., Neumann, R., et al., *Miner. Eng.* 22(4): 330(2009). https://doi.org/10.1016/j.mineng.2008.09.006.
29 Hamad, F., Pierscionek, B., and Bruun, H., *Meas. Sci. Technol.* 11: 1307(2000). https://doi.org/10.1088/0957-0233/11/9/308.
30. Raimundo, P., Cartellier, A., Beneventi, D., et al., *Chem. Eng. Sci.* 155: 504(2016). https://doi.org/10.1016/j.ces.2016.08.041.
31. Tayler, A., Holland, D., Sederman, A., et al., *Chem. Eng. Sci.* 71: 468(2012). https://doi.org/10.1016/j.ces.2011.11.014.
32. Atenas, M., Clark, M., and Lazarova, V., 15(4): 191(1998). https://doi.org/10.1002/(SICI)1521-4117(199808)15:4<191::AID-PPSC191>3.0.CO;2-4.
33. Ventura-Medina, E. and Cilliers, J., *Miner. Eng.* 13(3): 265(2000). https://doi.org/10.1016/S0892-6875(00)00006-6.
34. Kopra, R., Mutikainen, H., and Dahl, O., *TAPPI J.* 17(6): 343(2018). https://doi.org/10.32964/TJ17.06.343.
35. Imaichi, K. and Ohmi, K., *J. Fluid Mech.* 129: 283(1983). https://doi.org/10.1017/S0022112083000774.
36. Oberdier, L., *ASTM International* (848): 123(1984). https://doi.org/10.1520/STP32621S.
37. Chigier, N., *Prog. Energy Combust. Sci.* 17(3): 211(1991). https://doi.org/10.1016/0360-1285(91)90011-B.
38. Ow, C. and Crane, R., *Int. J. Heat Fluid Flow* 2(1): 47(1980). https://doi.org/10.1016/0142-727X(80)90008-9.
39. Sarker, D.K., Bertrand, D., Chtioui, Y., et al., *J. Texture Stud.* 29: 15(1998). https://doi.org/10.1111/j.1745-4603.1998.tb00151
40. Lecuona, A., Sosa, P.A., Rodriguez, P.A., et al., *Meas. Sci. Technol.* 11(8): 1152(2000). https://doi.org/10.1088/0957-0233/11/8/309.
41. Nishino, K., Hiroyuki, K., and Kahoru, T., *Meas. Sci. Technol.* 11(6): 633(2000). https://doi.org/10.1088/0957-0233/11/6/306.
42. Zabulis, X., Papara, M., Chatziargyriou, A., et al., *Colloids Surf., A* 309(1-3): 96(2007). https://doi.org/10.1016/j.colsurfa.2007.01.007.
43. Lappalainen, T. and Lehmonen, J., *Nord. Pulp Pap. Res. J.* 27(05): 930(2012). https://doi.org/10.3183/npprj-2012-27-05-p930-939.
44. Gaillard, T., Honorez, C., Jumeau, M., et al., *Colloids Surf., A* 473: 68(2015). https://doi.org/10.1016/j.colsurfa.2015.01.089.
45. Grau, R. and Heiskanen K., *Miner. Eng.* 15(7): 507(2002). https://doi.org/10.1016/S0892-6875(02)00074-2.
46. Bröder, D. and Sommerfeld, M., *Meas. Sci. Technol.* 18: 2513(2007). https://doi.org/10.1088/0957-0233/18/8/028.
47. Haapala, A., Honkanen, M., Liimatainen, H., et al., *WIT Trans. Eng. Sci.* 63: 343(2009). https://doi.org/10.2495/MPF090291.
48. Honkanen, M., Eloranta, H., and Saarenrinne, P., *Flow Meas. Instrum.* 21(1): 25(2010). https://doi.org/10.1016/j.flowmeasinst.2009.11.001.
49. Besagni, G. and Inzoli, F., *Exp. Therm. Fluid Sci.* 74: 27(2016). https://doi.org/10.1016/j.expthermflusci.2015.11.020.
50. Gulden, S., Riedele, C., Rollié, S., et al., *Chem. Eng. Sci.* 185: 168(2018). https://doi.org/10.1016/j.ces.2018.04.009.
51. Lichti, M. and Bart, H.-J., *Flow Meas. Instrum.* 60: 164(2018). https://doi.org/10.1016/j.flowmeasinst.2018.02.020.
52. Lioumbas, J., Georgiou, E., Kostoglou, M., et al., *Colloids Surf., A* 487: 92(2015). https://doi.org/10.1016/j.colsurfa.2015.09.050.
53. Drenckhan, W. and Hutzler, S., *Adv. Colloid Interface Sci.* 224: 1(2015). https://doi.org/10.1016/j.cis.2015.05.004.
54. Vega, E., Montanero, M., and Fernández, J., *Exp. Fluids* 47(2): 251(2009). https://doi.org/10.1007/s00348-009-0657-y.
55. Kowalczuk, P. and Drzymala, J., *Part. Sci. Technol.* 34(6): 645(2016) https://doi.org/10.1080/02726351.2015.1099582.